PHYSICAL REVIEW C **92**, 044313 (2015)

Microscopic evaluation of the hypernuclear chart with Λ hyperons

E. Khan,[1] J. Margueron,[2] F. Gulminelli,[3] and Ad. R. Raduta[4]
[1]*Institut de Physique Nucléaire, Université Paris-Sud, IN2P3-CNRS, F-91406 Orsay cédex, France*
[2]*Institut de Physique Nucléaire de Lyon, Université Claude Bernard Lyon 1, IN2P3-CNRS, F-69622 Villeurbanne cédex, France*
[3]*CNRS/ENSICAEN/LPC/Université de Caen Basse Normandy, UMR6534, F-14050 Caen cédex, France*
[4]*IFIN-HH, Bucharest-Magurele, POB-MG6, Romania*

(Received 28 May 2015; revised manuscript received 3 September 2015; published 16 October 2015)

Background: A large number of hypernuclei, where a considerable fraction of nucleons is replaced with strange baryons, and even pure hyperonic species are expected to be bound. However, the hypernuclear landscape remains largely unknown because of scarce constraints on the NY and YY interactions.
Purpose: We want to estimate the number of potentially bound hypernuclei. To evaluate realistic error bars within the theoretical uncertainties associated with the spherical mean-field approach and the present information from already synthesized hypernuclei on the N-Y and Y-Y channels, we limit ourselves to purely Λ hypernuclei, to magic numbers of Λ's (for $Z \leqslant 120$ and $\Lambda \leqslant 70$), and to even-even-even systems.
Method: We consider a density-functional approach adjusted to microscopic Bruckner-Hartree-Fock calculations, where the ΛΛ term is corrected in a phenomenological way, to reproduce present experimental constraints. Different models which strongly deviate at large densities, but giving the same bond energy, are generated to take into account the uncertainties related to the high-density equation of state.
Results: The number of bound even-even-even Λ hypernuclei is estimated to 491 680 ± 34 400. This relatively low uncertainty is attributable to the fact that the well-constrained low-density and highly unconstrained high-density behavior of the energy functional turn out to be largely decoupled. Results in Λ hypernuclei appear to be almost independent of the choice for the high-density part of the ΛΛ interaction. The location of the Λ hyperdriplines is also evaluated. Significant deviations from iron-nickel elements can be found for Λ hypernuclei with the largest binding energy per baryon. Proton, neutron, and Λ-hyperon magicity evolution and triple magic Λ hypernuclei are studied. Possible bubble and halo effects in Λ hypernuclei are also discussed.
Conclusions: The present results provide a first microscopic evaluation of the Λ-hypernuclear landscape. They shall benefit from the more and more accurate design of the Λ-based functionals. The measurements of Λ and multi-Λ hypernuclei together with additional constraints of the ΞΛ and ΞΞ interaction are mandatory to improve such critical information.

DOI: 10.1103/PhysRevC.92.044313 PACS number(s): 21.80.+a, 21.60.Jz, 21.10.Dr, 21.30.Fe

I. INTRODUCTION

The study of hypernuclei benefited from a great scientific interest since the 1960s [1,2]. Various hyperon-nucleus interaction [3], Skyrme Hartree-Fock [4–11], relativistic mean-field [12–19], generalized liquid drop [20–24] and, G matrix [25–27] models have been considered to underpin the hyperon-nucleon interaction from hypernuclei, to test the existence of bound hypernuclei, the stability of nucleonic cores against hyperon addition, or the occurrence of exotic pure strange systems or halo structures. With the advent of new dedicated experimental programs such as Japan Proton Accelerator Research Complex in Japan or proton antiproton detector array at GSI Facility for Antiproton and Ion Research, the study of the hypernuclei structure enjoys a revived interest [28–30].

Present facilities can only produce single- and double-Λ hypernuclei in a limited domain of mass. However, a general understanding of the specificity of hypernuclear structure with respect to nuclear structure requires the evaluation of the global hypernuclear chart, with strangeness as the third dimension [22,31]. Some recent works [29,30] address this problem within phenomenological mean-field models. However, the uncertainties on the hypernuclear chart associated with the choice of the functional in the strangeness sector are difficult to evaluate, because present experimental data on hypernuclei are scarce, and therefore a large arbitrariness is associated with the modeling of the hyperonic energy functional. To minimize such uncertainties, it is important to use as much as possible microscopically founded energy functionals from Brueckner or Dirac-Brueckner calculations, as well as the few available experimental data. The present work is an attempt in that direction.

The regular nuclear landscape, including an estimation of the uncertainties on its limits defined by the driplines, has been only recently microscopically studied [32], owing to the growth of calculation capacities. This is also attributable to the recent use of evaluation methods [33,34] for the uncertainties generated by the only input of such microscopic calculations: the nucleon-nucleon (NN) energy functional. The resulting uncertainty on the number of bound nuclei is typically of the order of 7% [32].

The present work aims to generalize such a study by designing the limits of the Λ-hypernuclear landscape and evaluating the uncertainties associated with the limited empirical information on the hyperonic functionals. For this purpose microscopic calculations of nuclei and Λ hypernuclei are performed using the energy density functional approach. We use a Skyrme functional optimized on nuclear physics data for the NN channel, while ΛN and $\Lambda\Lambda$ functionals fitted on microscopic Brueckner-Hartree-Fock (BHF) calculations are used, with modifications to take into account Λ-hypernuclei data constraints.

When dealing with a multistrange system, a very important issue is the possible presence of hyperons other than Λ. In particular, it was recognized since the early 1990s [16,18,35] that the $\Lambda + \Lambda \to \Xi + N$ decaying channel could play a major role in multistrange systems, because of the attractive character of the Ξ potential in nuclear matter, which could lead to the appearance of Ξ hyperons already for a strangeness number $|S| > 8$. The present most accepted value for the Ξ potential in symmetric nuclear matter $V_\Xi = -14$ MeV [36] is much less attractive than the value proposed in those earlier works [18], which pushes the Λ number threshold for Ξ contribution farther in strangeness. Moreover, it is clear that the contribution of Ξ will crucially depend on the Ξ-Ξ and Ξ-Λ interactions, which are presently completely unconstrained. The inclusion or removal of the Fock term in relativistic approaches seams to have, as well, an effect on the appearance the various kinds of hyperons in uniform matter [37]. Because of these uncertainties, we have chosen to limit ourselves to Λ hypernuclei in this work because Λ's are the only hyperons to be (relatively) constrained by experimental data.

Section II details the energy-density functional used, focusing on the way to design the $\Lambda\Lambda$ component. Section III is devoted to the determination of the corresponding parameters of the $\Lambda\Lambda$ functional. The Hartree-Fock calculations for Λ hypernuclei are performed in Sec. IV. Because in the hyperonic channel the spin-orbit interaction is expected to be very weak [38], the Λ-hypernuclear charts, location of the Λ hyperdriplines, and the estimation of the number of bound even-even-even Λ hypernuclei are evaluated for hypernuclear number $\Lambda = 0$, 2, 8, 20, 40, and 70. In Sec. V, the gross properties of Λ-hypernuclear structure are analyzed, namely the evolution of the energy per baryon as a function of the ΛN and $\Lambda\Lambda$ functionals. A study of magicity evolution in Λ hypernuclei, as well as of possible bubble and halo effects is also undertaken. Finally, Appendix A details the link between the bond energy and the $\Lambda\Lambda$ functional, whereas Appendix B provides an update of the strangeness analog resonances in multihyperon Λ hypernuclei.

II. DENSITY-FUNCTIONAL THEORY FOR Λ-HYPERNUCLEAR MATTER AND Λ HYPERNUCLEI

We consider a nonrelativistic system composed of interacting nucleons N and Λ's. The total Hamiltonian reads

$$\hat{H} = \hat{T}_N + \hat{T}_\Lambda + \hat{H}_{NN} + \hat{H}_{\Lambda\Lambda} + \hat{H}_{N\Lambda}, \tag{1}$$

where $\hat{T}_A$ is the kinetic energy operator and $\hat{H}_{AB}$ the interaction operator acting between A and B ($=N$ and Λ). We work in the mean-field approximation, where the ground state of the system is given by the tensor product, $|\Phi_N\rangle \otimes |\Phi_\Lambda\rangle$, where $|\Phi_N\rangle = \Pi_i a_i^+|-\rangle$ is a Slater determinant of nucleon states and $|\Phi_\Lambda\rangle = \Pi_\lambda a_\lambda^+|-\rangle$ is a Slater determinant of Λ states. The total Hamiltonian (1) can be expressed in terms of the nucleons (i) and λ states as

$$\hat{H} = \sum_i \hat{t}_i + \sum_\lambda \hat{t}_\lambda + \frac{1}{2}\sum_{i,j} \hat{v}_{ij}^{NN} + \frac{1}{2}\sum_{\lambda,\mu} \hat{v}_{\lambda\mu}^{\Lambda\Lambda} + \sum_{\lambda,i} \hat{v}_{i\lambda}^{N\Lambda}. \tag{2}$$

In the following, we consider the density-functional theory which allows relating in a direct way the BHF predictions for uniform matter to the properties of hypernuclei.

A. Energy-density functional deduced from BHF

In the present study of Λ hypernuclei and nuclear matter we use a density functional which has been determined directly from BHF theory including nucleons and Λ hyperons [26,27]. The total energy density $\epsilon(\rho_N,\rho_\Lambda)$ is related to the energy per particle calculated within the BHF framework, e_{BHF}, as $\epsilon(\rho_N,\rho_\Lambda) = (\rho_N + \rho_\Lambda)e_{\mathrm{BHF}}(\rho_N,\rho_\Lambda)$ and is decomposed in different terms,

$$\epsilon(\rho_N,\rho_\Lambda) = \frac{\hbar^2}{2m_N}\tau_N + \frac{\hbar^2}{2m_\Lambda}\tau_\Lambda + \epsilon_{NN}(\rho_N) + \epsilon_{N\Lambda}(\rho_N,\rho_\Lambda) + \epsilon_{\Lambda\Lambda}(\rho_\Lambda), \tag{3}$$

where, in infinite nuclear matter, the kinetic energy densities τ_N and τ_Λ are simple functions of the matter density: $\tau_i = \frac{3}{5}(6\pi^2/g_i)^{2/3}\rho_i^{5/3}$, with $g_i = 4(2)$ for $i = N(\Lambda)$.

In the nucleon sector, we use the SLy5 parametrization of the phenomenological Skyrme functional including nonlocal and spin-orbit terms, because it can correctly reproduce the properties of stable and exotic nuclei [39]. In the case of the strangeness sector, the spin-orbit interaction is known to be small [38] and is therefore neglected. The local density dependence of the $N\Lambda$ component of the energy density, $\epsilon_{N\Lambda}(\rho_N,\rho_\Lambda)$, is solely adjusted to the BHF predictions. To pin down the $N\Lambda$ coupling, the following energy density is defined: $(\rho_N + \rho_\Lambda)e_{\mathrm{BHF}}(\rho_N,\rho_\Lambda) - \rho_N e_{\mathrm{BHF}}(\rho_N,0) - \rho_\Lambda e_{\mathrm{BHF}}(0,\rho_\Lambda)$, where $e_{\mathrm{BHF}}(\rho_N,\rho_\Lambda)$ is the BHF energy per baryon in an infinite hypernuclear matter calculation. It is parametrized in terms of the nucleon and hyperon densities as Refs. [26,27],

$$\epsilon_{N\Lambda}(\rho_N,\rho_\Lambda) = -f_1(\rho_N)\rho_N\rho_\Lambda + f_2(\rho_N)\rho_N\rho_\Lambda^{5/3}, \tag{4}$$

where the first term physically corresponds to the attractive $N\Lambda$ interaction, corrected by the presence of the medium given by the function f_1, and the second term is induced by the repulsive momentum-dependent term of the Λ potential (considering the low-momentum quadratic approximation), also corrected by the medium through the function f_2. In the presence of the attractive $\Lambda\Lambda$ interaction, the term $\epsilon_{\Lambda\Lambda}$ is solely determined by the hyperon density as Ref. [27]

$$\epsilon_{\Lambda\Lambda}(\rho_\Lambda) = -f_3(\rho_\Lambda)\rho_\Lambda^2. \tag{5}$$

The functions f_i are given by the polynomial forms,

$$f_1(\rho_N) = \alpha_1 - \alpha_2\rho_N + \alpha_3\rho_N^2, \tag{6}$$

$$f_2(\rho_N) = \alpha_4 - \alpha_5\rho_N + \alpha_6\rho_N^2, \tag{7}$$

$$f_3(\rho_\Lambda) = \alpha_7 - \alpha_8\rho_\Lambda + \alpha_9\rho_\Lambda^2. \tag{8}$$

In principle, the functions f_1 and f_2 depend on the densities ρ_N and ρ_Λ associated with conserved charges in the medium. However, because nucleons are the dominant species, even in the presence of Λ's, the dependence on ρ_Λ is neglected in these functions. In the case of f_3, it trivially depends on ρ_Λ only, because it impacts the part of the functional referring to pure Λ matter.

Different $N\Lambda$ potentials have been parametrized which fit equally well the scarce $N\Lambda$ phase shifts; see, for instance, discussion and references in Ref. [40]. The present study is based on three of them for which a density functional has been derived, based on BHF predictions [26,27], namely DF-NSC89, DF-NSC97a, and DF-NSC97f. The functional DF-NSC89 is based on the Nijmegen soft-core potential NSC89 [41], while the functionals DF-NSC97a and DF-NSC97f are based on two of a series of six different hyperon-nucleon potentials which equally well reproduce the measured scattering lengths in the ΛN and ΣN channels and correspond to different values of the magnetic vector meson ratio α, which cannot be constrained by the phase-shift information [42,43].

Although more recent functionals have been parametrized [40], by adding, for instance, isospin degree of freedom, the functionals considered in this study already represent a good sample of the uncertainty generated by the lack of empirical information in the strangeness sector. This affects microscopic approaches like BHF [8,26,27], although to a lesser extent than fully phenomenological mean-field models [6,7,9–11,15–18,25,28–30]. Indeed, the models DF-NSC97a and DF-NSC97f correspond to the two extreme choices for the unconstrained α parameter [42,43], leading to the softest and stiffest equation of state, respectively. It should be noted that no experimental information is available on Λ-Λ scattering, meaning that these phenomenological bare interactions are completely unconstrained in the Λ-Λ channel. For this reason, NSC89 does not contain any Λ-Λ interaction. The NSC97 models assume for this channel a simple SU(3) extension of the original Nijmegen potential models to multiple strangeness $S = -2$. The values for the parameters $\alpha_1 - \alpha_9$ of the functions $f_1 - f_3$ are given in Table I for the functionals DF-NSC89, DF-NSC976a, and DF-NSC97f.

The single-particle energies in uniform matter are deduced from the energy functional (3), as $e_N^{\mathrm{unif}}(k) = \frac{\hbar^2 k^2}{2m_N} + v_N^{\mathrm{unif}}$ and $e_\Lambda^{\mathrm{unif}}(k) = \frac{\hbar^2 k^2}{2m_\Lambda} + v_\Lambda^{\mathrm{unif}}$, where

$$v_N^{\mathrm{unif}}(\rho_N,\rho_\Lambda) = v_N^{\mathrm{Sky}} + \frac{\partial \epsilon_{N\Lambda}}{\partial \rho_N}, \tag{9}$$

TABLE I. Parameters of the f_i functions [see Eqs. (6)–(8)] for the functionals DF-NSC89, DF-NSC97a, and DF-NSC97f.

Force	α_1	α_2	α_3	α_4	α_5	α_6	α_7	α_8	α_9
DF-NSC89 [26,27]	327	1159	1163	335	1102	1660	0	0	0
DF-NSC97a [27]	423	1899	3795	577	4017	11 061	38	186	22
DF-NSC97f [27]	384	1473	1933	635	1829	4100	50	545	981

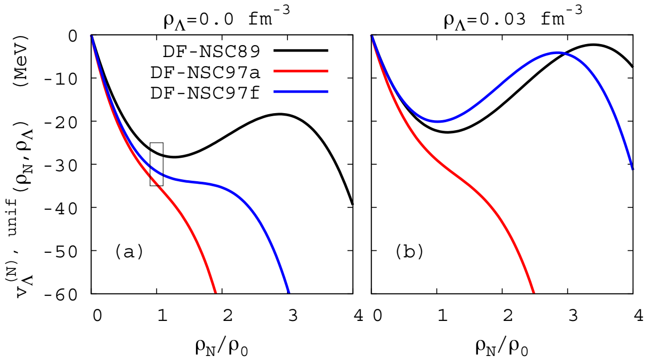

FIG. 1. (Color online) Potential $v_\Lambda^{(N),\mathrm{unif}}(\rho_N,\rho_\Lambda)$ as a function of the nucleon density ρ_N (in units of the saturation density ρ_0) for the functionals DF-NSC89, DF-NSC97a, and DF-NSC97f without Λ (a) and with $\rho_\Lambda = 0.03$ fm^{-3} (b).

v_N^{Sky} being deduced from the Skyrme functional [44,45], and

$$v_\Lambda^{\mathrm{unif}}(\rho_N,\rho_\Lambda) = \frac{\partial \epsilon_{N\Lambda}}{\partial \rho_\Lambda} + \frac{\partial \epsilon_{\Lambda\Lambda}}{\partial \rho_\Lambda}. \tag{10}$$

In the following, the hyperon potential $v_\Lambda^{\mathrm{unif}}$ is decomposed into two terms, $v_\Lambda^{\mathrm{unif}} = v_\Lambda^{(N),\mathrm{unif}} + v_\Lambda^{(\Lambda),\mathrm{unif}}$ using Eqs. (4) and (5),

$$v_\Lambda^{(N),\mathrm{unif}} = \frac{\partial \epsilon_{N\Lambda}}{\partial \rho_\Lambda} = -f_1(\rho_N)\rho_N + \frac{5}{3} f_2(\rho_N)\rho_N\rho_\Lambda^{2/3} \tag{11}$$

$$v_\Lambda^{(\Lambda),\mathrm{unif}} = \frac{\partial \epsilon_{\Lambda\Lambda}}{\partial \rho_\Lambda} = -2\alpha_7\rho_\Lambda + 3\alpha_8\rho_\Lambda^2 - 4\alpha_9\rho_\Lambda^3. \tag{12}$$

The term $v_\Lambda^{(N),\mathrm{unif}}$ stands for the contribution of the nucleons to the hyperon potential, while the term $v_\Lambda^{(\Lambda),\mathrm{unif}}$ represents the direct contribution of the hyperons to their own potential. The properties of the potential $v_\Lambda^{(N),\mathrm{unif}}$ are analyzed in Fig. 1, imposing $\rho_n = \rho_p$. In the left panel, the potential $v_\Lambda^{(N),\mathrm{unif}}$ is displayed without Λ particles, while in the right panel a small amount of Λ is considered, corresponding to a representative average Λ density in single-Λ hypernuclei (see Sec. III A). It is expected, from experimental single-Λ-hypernuclei data, that the potential $v_\Lambda^{(N)}$ is about −30 MeV at saturation density [26]. This empirical condition is satisfied for the three functionals—DF-NSC89, DF-NSC97a, and DF-NSC97f—at saturation density, as shown on the left panel of Fig. 1. For a fixed and small amount of Λ, the potential $v_\Lambda^{(N),\mathrm{unif}}$ is attractive at large densities for all the functionals, owing to the α_3 term in the function f_1. Already in the late 1980s it was clear that some repulsion is necessary at high densities to explain hypernuclear data [3]. For a finite amount of Λ, the α_6 term in function f_2 gives a repulsive contribution and can compensate the attractive α_3 term if $\rho_\Lambda > (\frac{3}{5}\frac{\alpha_3}{\alpha_6})^{3/2}$. For the functionals DF-NSC89, DF-NSC97a, and DF-NSC97f, this occurs for $\rho_\Lambda >$ 0.27, 0.09, and 0.15 fm^{-3}, respectively. These substantially different numbers reveal the large uncertainties at high density in the predictions of the considered functionals. These three functionals have been used before in Skyrme-Hartree-Fock calculations of single-Λ hypernuclei from C to Pb, and the resulting Λ single-particle levels have been confronted in detail to experimental data [27]. The single-particle levels of the heaviest Λ hypernuclei, which should, in principle, be reasonably well described in a mean-field calculation, were seen to be systematically overbound by DF-NSC97a and slightly underbound by DF-NSC89, while DF-NSC97f nicely reproduces the data. In this sense, we can consider that the Λ potentials in uniform matter $v_\Lambda^{(N),\mathrm{unif}}$ presented in Fig. 1 span the range compatible with Λ-hypernuclear data, even if the functionals appear to be probably too attractive at high density [27].

These functionals have also been extended to other hyperonic channels, namely Σ and Ξ, assuming SU(3) symmetry, and exploited in BHF matter calculations [46]. However, these extrapolations of the $N-\Lambda$ channel to the rest of the octet have been severely questioned in recent years owing to the difficulty of standard functionals to predict the existence of very massive neutron stars [47,48]. For this reason we do not consider these extensions here. It is, however, interesting to note that all functionals predict that, for a sufficiently high number of Λ, the $\Lambda + \Lambda \to \Xi + N$ decay channel should open and Ξ should contribute to the multistrange nuclei. The threshold Λ fraction for Ξ appearance is estimated to be $\rho_\Lambda/\rho_N = 0.17$ for DF-NSC89, the only functional that predicts a Ξ potential in symmetric matter $V_\Xi = -15$ MeV [27], compatible with experimental data [36]. It should be noted that this criterion is largely influenced by the value of the Ξ potential in symmetric matter, as expected, because, for instance, the threshold Λ fraction for Ξ appearance is estimated to be $\rho_\Lambda/\rho_N = 0.15$ and 0.08 fm^{-3} for the DF-NSC97a and DF-NSC97f functionals having more attractive Ξ potentials [27].

This means that the results we get for highly strange Λ hypernuclei have to be taken with caution. In particular, driplines associated with a Λ fraction $\rho_\Lambda/\rho_N = 0.17$ have to be considered as a lower bound, because even more strangeness would be compatible with bound systems if Ξ would be accounted for.

The two terms $v_\Lambda^{(N),\mathrm{unif}}$ and $v_\Lambda^{(\Lambda),\mathrm{unif}}$ contributing to the potential $v_\Lambda^{\mathrm{unif}}$ [Eq. (10)] are compared in Fig. 2, as a function of the nucleonic density ρ_N and for different proportions of Λ. As expected, for a sufficiently large amount of Λ, the term $v_\Lambda^{(N),\mathrm{unif}}$ becomes repulsive at high nucleonic density. At low density the functionals DF-NSC97a and DF-NSC97f predict very close potentials $v_\Lambda^{(\Lambda),\mathrm{unif}}$, but as the nucleonic density increases the predictions of these two functionals increasingly deviate. Because the dominant term in α_9 is attractive, the potential $v_\Lambda^{(\Lambda),\mathrm{unif}}$ will finally curve down at very high densities, but this occurs in physical situations which will be hardly met in nature. Indeed, for the functional DF-NSC97a, the potential continuously increases up to $\rho_N \approx 10\rho_0$ and for a fraction of hyperons $\leqslant 50\%$. For DF-NSC97f, the effect of α_9 is already curving down the potential for $\rho_N \approx 8\rho_0$ and 20% of Λ. In pure Λ matter, the potential $v_\Lambda^{(\Lambda),\mathrm{unif}}$ becomes repulsive between $\rho_0/2$ and ρ_0. The functional DF-NSC97f predicts also a decreasing potential starting from $1.5\rho_0$, while this behavior is pushed to much larger values (beyond $20\rho_0$) with DF-NSC97a.

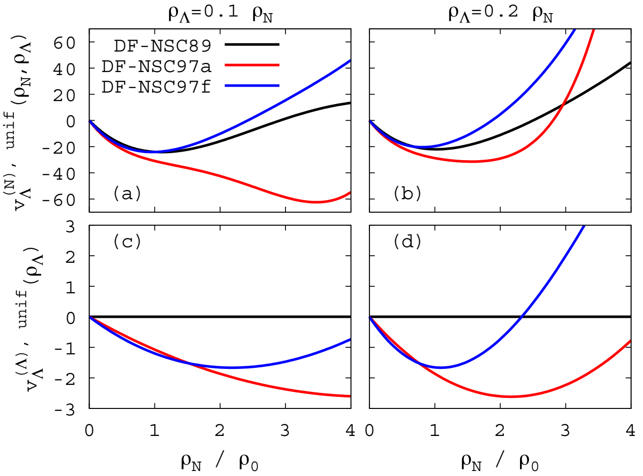

FIG. 2. (Color online) Comparison of $v_\Lambda^{(N),\mathrm{unif}}$ (a),(b) and $v_\Lambda^{(\Lambda),\mathrm{unif}}$ (c),(d) as a function of the nucleon density ρ_N (in units of the saturation density ρ_0) for the functionals DF-NSC89, DF-NSC97a, and DF-NSC97f and a Λ fraction set to 10% (a),(c) and 20% (b),(d).

These differences between the functionals clearly show that the high-density properties of Λ hypermatter are largely unconstrained. From the phenomenological point of view, the existence of very massive neutron stars (about $2M_\odot$ [49]) requires a strongly repulsive $v_\Lambda^{\mathrm{unif}}$ potential at high density, which corresponds to a low value of the α parameter, in terms of the elementary Nijmegen interactions. In principle, the very existence of such massive stars could be used as an extra constraint for the functional, and was often considered in the relativistic mean-field literature (see, for instance, the recent work [19], and Refs. therein). However, owing to the presence of different hyperon species in the core of massive neutron stars, with highly unknown interaction couplings, it is not straightforward to convert this qualitative statement into a sharp constraint on the $v_\Lambda^{\mathrm{unif}}$ potential. More specifically, it should be noted that no BHF calculation is presently able to reproduce the empirical observation of $2M_\odot$ neutrons stars. This contradiction between our knowledge of supranuclear matter and observation is usually called the hyperonization puzzle [50].

Finally, it can be noted from Fig. 2 that the $v_\Lambda^{(\Lambda),\mathrm{unif}}$ term is much smaller than $v_\Lambda^{(N),\mathrm{unif}}$: $v_\Lambda^{(\Lambda),\mathrm{unif}}$ contributes to less than 10% to the total potential $v_\Lambda^{\mathrm{unif}}$. In the functionals DF-NSC97a and DF-NSC97f, the contribution of the term $v_\Lambda^{(\Lambda),\mathrm{unif}}$, induced by the $\Lambda\Lambda$ interaction, to the properties of hyperonic matter is therefore expected to be rather weak. As discussed above, this result might not be entirely physical, because the Λ-Λ interaction in the NSC97 models is not fitted on experimental data, but only extrapolated from the N-Λ interaction. The $\Lambda\Lambda$ term of the functional can thus be phenomenologically adjusted, as explained in the next section.

B. Phenomenological correction to the term $\epsilon_{\Lambda\Lambda}$

The term $\epsilon_{\Lambda\Lambda}$ defined by Eq. (5) is generated by the $\Lambda\Lambda$ interaction: Only the functionals DF-NSC97a and DF-NSC97f for which the $\Lambda\Lambda$ interaction has been included in the BHF calculation, have a nonzero $\epsilon_{\Lambda\Lambda}$ [26,27].

However, large uncertainties remain on the $\Lambda\Lambda$ interaction, as discussed above. The functionals introduced in Sec. II A, based on an SU(3) extrapolation of the N-Λ bare interaction to the $S = -2$ channel [41,43], do not lead to a satisfactory description of the binding energy of double-Λ hypernuclei [27], which is the only empirical information that we have on Λ-Λ couplings [51–53]. Moreover, Fig. 2 shows that, though the DF-NSC97a and DF-NSC97f functionals in the Λ-Λ channel are very similar at low density, they drastically differ above saturation. In view of the already-mentioned hyperonization puzzle, it is therefore reasonable to consider that an even larger uncertainty in the high-density behavior has to be associated with the term $\epsilon_{\Lambda\Lambda}$.

In the following, we therefore propose to modify the $\epsilon_{\Lambda\Lambda}$ term taking into account phenomenological arguments to deal with the uncertainty on the microscopic BHF results. In practice, the values of the $\alpha_7, \alpha_8, \alpha_9$ parameters of the original functional (3) are replaced with different values $\tilde{\alpha}_7, \tilde{\alpha}_8, \tilde{\alpha}_9$ defining the new $\tilde{\epsilon}_{\Lambda\Lambda}$ term,

$$\tilde{\epsilon}_{\Lambda\Lambda} = -\left(\tilde{\alpha}_7 - \tilde{\alpha}_8\rho_\Lambda + \tilde{\alpha}_9\rho_\Lambda^2\right)\rho_\Lambda^2, \tag{13}$$

and the new potential $\tilde{v}_\Lambda^{(\Lambda),\mathrm{unif}}$,

$$\tilde{v}_\Lambda^{(\Lambda),\mathrm{unif}} = -2\tilde{\alpha}_7\rho_\Lambda + 3\tilde{\alpha}_8\rho_\Lambda^2 - 4\tilde{\alpha}_9\rho_\Lambda^3. \tag{14}$$

The determination of these parameters is based on the following phenomenological prescription.

(i) Because the $\Lambda\Lambda$ interaction is expected to be repulsive at high density (to support, for instance, the observed $2M_\odot$ neutron stars), the coefficient $\tilde{\alpha}_9$ is taken as $\leqslant 0$.

(ii) A parameter x is introduced, which represents the Λ density (in units of the saturation density ρ_0), where the Λ potential in hyperonic matter $\tilde{v}_\Lambda^{(\Lambda),\mathrm{unif}}$ (14) changes its sign and becomes repulsive.

(iii) Finally, we impose a relation between the $\Lambda\Lambda$ interaction and the bond energy in ^{6}He, obtained from the local density approximation, which we discuss hereafter [27].

Condition (i) imposes $\tilde{\alpha}_9 \leqslant 0$. For convenience, we set $\tilde{\alpha}_9 = 0$, giving minimal repulsion. Figure 2 shows that the contribution of the term α_9 appears at very high densities which are certainly never reached in neutron stars.

Condition (ii) and Eq. (14) give

$$2\tilde{\alpha}_7 = 3\tilde{\alpha}_8\rho_\Lambda = 3\tilde{\alpha}_8 x\rho_0, \tag{15}$$

meaning that the parameter x controls the high-density behavior of Λ matter: the larger x, the softer the equation of state (EoS) with hyperons.

Condition (iii) is related to the bond energy $\Delta B_{\Lambda\Lambda}$, which is defined as [26,27]

$$\Delta B_{\Lambda\Lambda}(A) = -E\left({}^{A-2}Z\right) + 2E\left({}^{A-1}_{\Lambda}Z\right) - E\left({}^{A}_{\Lambda\Lambda}Z\right), \tag{16}$$

where ${}^{A-2}Z$ is a nucleus with no hyperon, ${}^{A-1}_{\Lambda}Z$ is a single-Λ hypernucleus, and ${}^{A}_{\Lambda\Lambda}Z$ is a double-Λ hypernucleus. It should be noted that, experimentally, ^{6}He and related hypernuclei provide the most accurate value of a bond energy, with $\Delta B_{\Lambda\Lambda} \simeq 1$ MeV [52,53].

The relation between the bond energy and the functional is derived in Appendix A, providing

$$\Delta B_{\Lambda\Lambda}(A) \approx -2\frac{\tilde{\epsilon}_{\Lambda\Lambda}[\rho_\Lambda(A)]}{\rho_\Lambda(A)}. \tag{17}$$

Injecting Eq. (13) into Eq. (17), the following relation is deduced:

$$2\rho_\Lambda(A)[\tilde{\alpha}_7 - \tilde{\alpha}_8\rho_\Lambda(A)] = \Delta B_{\Lambda\Lambda}(A). \tag{18}$$

Using Eq. (15) and introducing $x_\Lambda(A) = \rho_\Lambda(A)/\rho_0$, the average Λ density in double-Λ hypernucleus ${}^{A}_{\Lambda\Lambda}Z$, we obtain from Eq. (18),

$$[3x - 2x_\Lambda(A)]x_\Lambda(A)\rho_0^2\tilde{\alpha}_8 = \Delta B_{\Lambda\Lambda}(A). \tag{19}$$

We can thus express the new parameters $\tilde{\alpha}_7$ and $\tilde{\alpha}_8$ as a function of x,$x_\Lambda(A)$ and $\Delta B_{\Lambda\Lambda}(A)$ from Eqs. (15) and (19) as

$$\tilde{\alpha}_7 = \frac{3}{2}\frac{x\ \Delta B_{\Lambda\Lambda}(A)}{[3x - 2x_\Lambda(A)]x_\Lambda(A)\rho_0}, \tag{20}$$

$$\tilde{\alpha}_8 = \frac{\Delta B_{\Lambda\Lambda}(A)}{[3x - 2x_\Lambda(A)]x_\Lambda(A)\rho_0^2}. \tag{21}$$

The following expressions for the energy density and the potential are deduced from Eqs. (13) and (14):

$$\tilde{\epsilon}_{\Lambda\Lambda} = -\frac{\tilde{\alpha}_8}{2}\rho_\Lambda^2(3x\rho_0 - 2\rho_\Lambda), \tag{22}$$

$$\tilde{v}_\Lambda^{(\Lambda),\mathrm{unif}} = -3\tilde{\alpha}_8\rho_\Lambda(x\rho_0 - \rho_\Lambda). \tag{23}$$

Because the parameters $\tilde{\alpha}_7$ and $\tilde{\alpha}_8$ are linearly related to the bond energy, the energy density $\tilde{\epsilon}_{\Lambda\Lambda}$ also scales with the bond energy. The relation between $\tilde{\alpha}_7$ and $\tilde{\alpha}_8$ and the parameters x and x_Λ is more complicated. Let us consider the limit where $x \gg x_\Lambda$. In this case, the parameters $\tilde{\alpha}_7$ and $\tilde{\alpha}_8$ reduce to the simpler expressions:

$$\tilde{\alpha}_7^* = \frac{\Delta B_{\Lambda\Lambda}(A)}{2x_\Lambda(A)\rho_0} \quad \text{and} \quad \tilde{\alpha}_8^* = \frac{\Delta B_{\Lambda\Lambda}(A)}{3x x_\Lambda(A)\rho_0^2}. \tag{24}$$

It should be noted that $\tilde{\alpha}_7^*$ is independent of x, while $\tilde{\alpha}_8^*$ is inversely related to x. Therefore, the parameter $\tilde{\alpha}_8$ is mostly related to the prescription (ii), modifying the high-density part of the mean field, while $\tilde{\alpha}_7$ is almost independent of x. Moreover, at the limit $x \gg x_\Lambda$, the Λ potential at the density $\rho_\Lambda(A)$ is given by $\tilde{v}_\Lambda^{(\Lambda)}[\rho_\Lambda = x_\Lambda(A)\rho_0] \approx \tilde{v}_\Lambda^{(\Lambda)*}$, and the potential energy density is given by $\tilde{\epsilon}_{\Lambda\Lambda}[\rho_\Lambda = x_\Lambda(A)\rho_0] \approx \tilde{\epsilon}_{\Lambda\Lambda}^*$, where

$$\tilde{v}_\Lambda^{(\Lambda)*} = -\Delta B_{\Lambda\Lambda}(A), \tag{25}$$

$$\tilde{\epsilon}_{\Lambda\Lambda}^* = -0.5\Delta B_{\Lambda\Lambda}(A)x_\Lambda(A)\rho_0. \tag{26}$$

The parameter $\tilde{v}_\Lambda^{(\Lambda)*}$ is only related to the bond energy and is independent of x and $x_\Lambda(A)$, while the parameter $\tilde{\epsilon}_{\Lambda\Lambda}^*$ depends only on the bond energy and $x_\Lambda(A)$, independently of the value of x. At the limit where $x \gg x_\Lambda$, the potential and the energy density at $x_\Lambda(A)$ depends only on the bond energy and $x_\Lambda(A)$, and are independent of x. More generally,

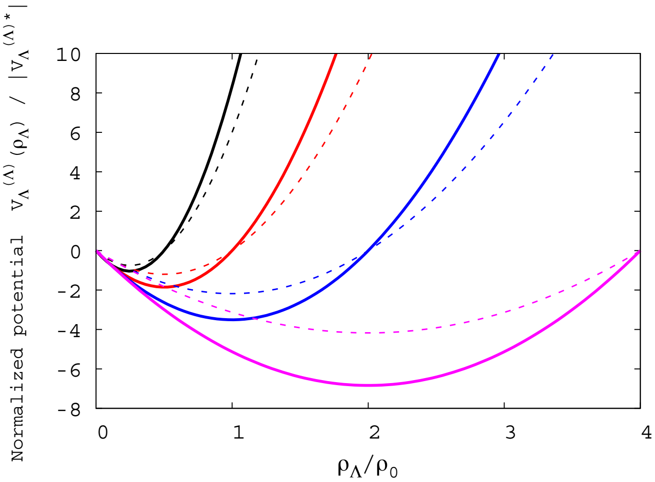

FIG. 3. (Color online) Normalized potential $V_\Lambda^{(\Lambda)}(\rho_\Lambda)/|V_\Lambda^{(\Lambda)*}|$ for several choices of x and x_Λ; see text.

the relations

$$\frac{\tilde{v}_\Lambda^{(\Lambda)}[\rho_\Lambda = x_\Lambda(A)\rho_0]}{|\tilde{v}_\Lambda^{(\Lambda)*}|} = -1 + \frac{1}{3}\frac{x_\Lambda}{x} + o\left[\left(\frac{x_\Lambda}{x}\right)^2\right], \tag{27}$$

$$\frac{\tilde{\epsilon}_{\Lambda\Lambda}[\rho_\Lambda = x_\Lambda(A)\rho_0]}{|\tilde{\epsilon}^*_{\Lambda\Lambda}|} = -1 + o\left[\left(\frac{x_\Lambda}{x}\right)^2\right], \tag{28}$$

hold, where the correction goes like $x_\Lambda(A)/x$.

Equations (27) and (28) show that the scaled $\Lambda\Lambda$ potential $\tilde{v}_\Lambda^{(\Lambda)}/\tilde{v}_\Lambda^{(\Lambda)*}$ and the scaled Λ energy $\tilde{\epsilon}_{\Lambda\Lambda}/\tilde{\epsilon}^*_{\Lambda\Lambda}$ solely depend on x and x_Λ and are independent of the bond energy. A complete representation of the parameter space can therefore be obtained by representing these scaled quantities as a function of the Λ density and largely varying only the two parameters x and x_Λ. These normalized potentials (respectively energies) are represented in Fig. 3 (Fig. 4).

According to condition (ii), the mean-field potential changes its sign for the density $\rho_\Lambda = x\rho_0$. This is well observed in Fig. 3. Therefore, the effect of increasing the parameter x makes the Λ mean-field potential and energy density softer. In a similar but weaker way, Figs. 3 and 4 show that the effect of the parameter x_Λ is to soften the mean-field potential and the energy density as x_Λ increases.

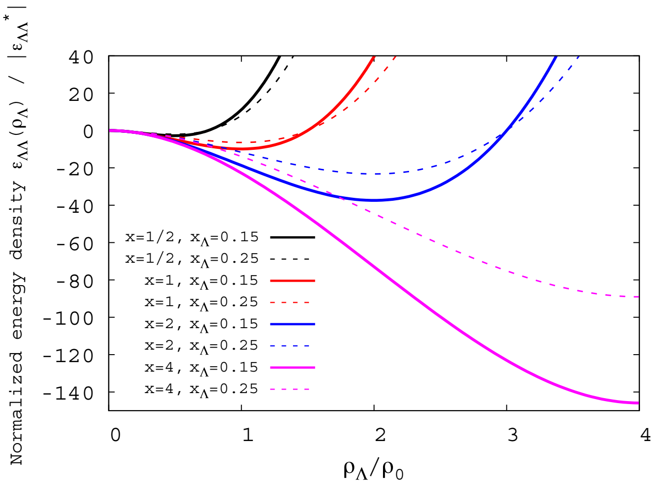

FIG. 4. (Color online) Normalized energy density $\epsilon_{\Lambda\Lambda}(\rho_\Lambda)/|\epsilon^*_{\Lambda\Lambda}|$ for the same parameters as in Fig. 3.

The potential and energy-density behavior, displayed in Figs. 3 and 4, show that this choice of parameters spans a wide range of qualitative behaviors of the energy functional.

C. Application of the energy-density functionals to Λ hypernuclei

For the sake of completeness, we recall here the results obtained in [26,27], also used in the present work, describing the implementation of the Hartree-Fock approach in the Λ-hypernuclear case. Nucleons and Λ's in the medium acquire an effective mass which is generated by the momentum dependence of the interaction. The description of finite nuclei requires disentangling the momentum-dependent part of the in-medium potential (the correction to the masses) from the momentum-independent one, hereafter called the local part. The local energy density is defined by

$$\frac{\hbar^2}{2m_N}\tau_N + \epsilon_{NN}(\rho_N) = \frac{\hbar^2}{2m_N^*(\rho_N)}\tau_N + \epsilon_{NN}^{\text{loc}}(\rho_N), \tag{29}$$

$$\frac{\hbar^2}{2m_\Lambda}\tau_\Lambda + \epsilon_{N\Lambda}(\rho_N,\rho_\Lambda) = \frac{\hbar^2}{2m_\Lambda^*(\rho_N)}\tau_\Lambda + \epsilon_{N\Lambda}^{\text{loc}}(\rho_N,\rho_\Lambda), \tag{30}$$

which can be recast as

$$\epsilon_{NN}^{\text{loc}} = \epsilon_{NN} - \frac{3\rho_N\hbar^2}{10}\left(\frac{6\pi^2\rho_N}{g_N}\right)^{2/3}\left(\frac{1}{m_N^*} - \frac{1}{m_N}\right), \tag{31}$$

$$\epsilon_{N\Lambda}^{\text{loc}} = \epsilon_{N\Lambda} - \frac{3\rho_\Lambda\hbar^2}{10}\left(\frac{6\pi^2\rho_\Lambda}{g_\Lambda}\right)^{2/3}\left(\frac{1}{m_\Lambda^*} - \frac{1}{m_\Lambda}\right), \tag{32}$$

where ϵ_{NN} is derived from the Skyrme functional [44,45] and $\epsilon_{N\Lambda}$ is given by Eq. (4). We have already seen that the nucleon contribution to the Λ potential, $\epsilon_{N\Lambda}$, is much bigger than the Λ contribution, $\epsilon_{\Lambda\Lambda}$. For this reason, the contribution of the $\Lambda\Lambda$ interaction to the Λ-effective mass can be considered as a small corrections, and it has been neglected in Ref. [27]. We can therefore write

$$\epsilon_{\Lambda\Lambda}^{\text{loc}}(\rho_\Lambda) = \epsilon_{\Lambda\Lambda}(\rho_\Lambda). \tag{33}$$

In Eqs. (31) and (32) the local part of the energy density requires the knowledge of the effective masses m_N^* and m_Λ^*. The nucleon-effective mass m_N^* is given from the Skyrme interaction [44,45]. The effective mass of the Λ particles is mainly generated by the momentum dependence of the $N\Lambda$ interaction, and it can be deduced from the BHF calculations. The result is expressed as a polynomial in the nucleonic density ρ_N as [26]

$$\frac{m_\Lambda^*(\rho_N)}{m_\Lambda} = \mu_1 - \mu_2\rho_N + \mu_3\rho_N^2 - \mu_4\rho_N^3. \tag{34}$$

The values for the parameters μ_{1-4} for the functional considered here are given in Table II and the density dependence of the effective mass is shown in Fig. 5. Because the effective mass is only necessary in the description of finite nuclei, we

TABLE II. Parameters of the Λ-effective mass given by Eq. (34) for the functionals considered in this paper.

Force	μ_1	μ_2	μ_3	μ_4
DF-NSC89 [26,27]	1	1.83	5.33	6.07
DF-NSC97a [27]	0.98	1.72	3.18	0
DF-NSC97f [27]	0.93	2.19	3.89	0

have limited the densities to values around saturation densities in Fig. 5. We can again observe, on the left panel, that the three functionals show a qualitatively similar behavior for the Λ-effective mass at low density, with the stiffest model DF-NSC97f showing, as expected, the strongest momentum dependence.

Given the functional form of ϵ^{loc} and m^* for the nucleons and the Λ's, Eq. (3) can be rewritten in a form which explicitly disentangles the terms coming from the local operator $\hat{\rho}$ and the nonlocal operator $\hat{\tau} = \vec{\nabla}\hat{\rho}\vec{\nabla}$ as

$$\epsilon(\rho_N,\rho_\Lambda,\tau_N,\tau_\Lambda) = \frac{\hbar^2}{2m_N^*(\rho_N)}\tau_N + \frac{\hbar^2}{2m_\Lambda^*(\rho_N)}\tau_\Lambda + \epsilon_{NN}^{\text{loc}}(\rho_N) + \epsilon_{N\Lambda}^{\text{loc}}(\rho_N,\rho_\Lambda) + \epsilon_{\Lambda\Lambda}(\rho_\Lambda). \tag{35}$$

Minimizing the total energy, defined from the density functional (35), and using the Skyrme model for the nucleonic part, we obtain the usual Schrödinger equation ($i = N,\Lambda$),

$$\left[-\nabla\frac{\hbar^2}{2m_i^*(r)}\nabla + V_i(r) - iW_i(r)(\nabla\times\sigma)\right]\varphi_{i,\alpha}(r) = -e_{i,\alpha}\varphi_{i,\alpha}(r), \tag{36}$$

where the nucleon potential V_N is defined as

$$V_N(r) = v_N^{\text{unif}}(r) + \frac{\partial}{\partial\rho_N}\left[\frac{m_\Lambda}{m_\Lambda^*(\rho_N)}\right] \times \left[\frac{\tau_\Lambda}{2m_\Lambda} - \frac{3}{5}\frac{(3\pi^2)^{2/3}\hbar^2}{2m_\Lambda}\rho_\Lambda^{5/3}\right]. \tag{37}$$

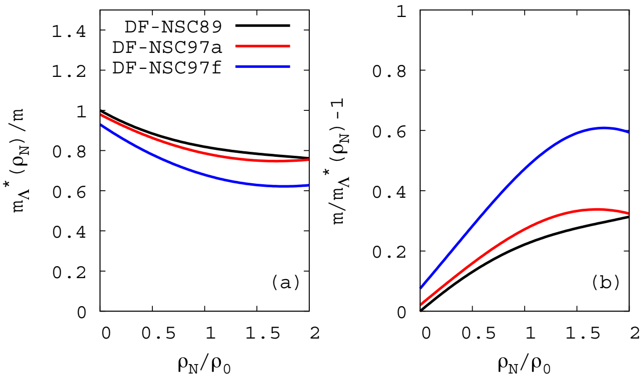

FIG. 5. (Color online) Ratio of the effective and bare Λ mass $m_\Lambda^*(\rho_N)/m_\Lambda$ (a) and $1 - m_\Lambda/m_\Lambda^*$ (b) as a function of the nucleon density ρ_N (in units of the saturation density ρ_0) for the functionals DF-NSC89, DF-NSC97a, and DF-NSC97f.

The hyperon potential V_Λ is given by

$$V_\Lambda(r) = v_\Lambda^{\text{unif}} - \left[\frac{m_\Lambda}{m_\Lambda^*(\rho_N)} - 1\right]\frac{(3\pi^2)^{2/3}\hbar^2}{2m_\Lambda}\rho_\Lambda^{2/3}. \tag{38}$$

As in the uniform case, the hyperon potential V_Λ is decomposed into two terms, $V_\Lambda = V_\Lambda^{(N)} + V_\Lambda^{(\Lambda)}$, where

$$V_\Lambda^{(N)}(r) = v_\Lambda^{(N),\text{unif}} - \left[\frac{m_\Lambda}{m_\Lambda^*(\rho_N)} - 1\right]\frac{(3\pi^2)^{2/3}\hbar^2}{2m_\Lambda}\rho_\Lambda^{2/3}, \tag{39}$$

$$V_\Lambda^{(\Lambda)}(r) = v_\Lambda^{(\Lambda),\text{unif}}. \tag{40}$$

The factor $[m_\Lambda/m_\Lambda^*(\rho_N) - 1]$ in Eq. (39) is displayed on the right panel of Fig. 5, showing that it is quite large around saturation density, between 0.2 and 0.5. The modification of the Λ potential in nuclei with respect to the uniform potential can be quite important as it scales approximately with the kinetic energy density of the Λ's.

III. DETERMINATION OF THE $\Lambda\Lambda$ FUNCTIONAL

In the following we use the previous formalism to perform calculations in finite nuclei and to determine the parameters of the $\Lambda\Lambda$ functional. In the case of single-Λ-hypernuclei, there is no $\Lambda\Lambda$ interaction, and the corresponding terms in the functional shall therefore not be considered. We therefore set $\epsilon_{\Lambda\Lambda} = 0$ for single-Λ-hypernuclei, while for double- and many-Λ-hypernuclei, we consider the original expression (5) for $\epsilon_{\Lambda\Lambda}$.

A. The average Λ density in hypernuclei

According to Eq. (17), the bond energy and the average density in the double-Λ hypernucleus ${}^{A}_{\Lambda\Lambda}Z$ are closely related. The bond energy can be experimentally constrained, but no experimental determination of the average Λ density exists yet. Figure 6 displays the nucleon and Λ densities in ${}^{5}_{\Lambda}$He and ${}^{6}_{\Lambda\Lambda}$He for the functionals DF-NSC89, DF-NSC97a, and DF-NSC97f, using SLy5 for the nucleons. The average single-

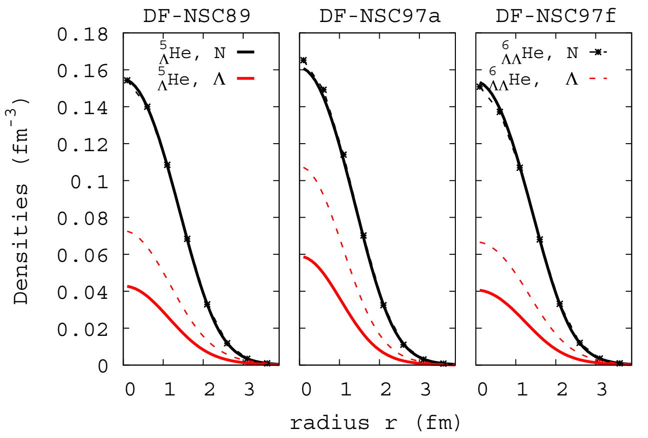

FIG. 6. (Color online) Density profiles in ^{4}He isotopes with the addition of one or two Λ hyperons. Black (red) lines, nucleon (Λ) density; solid (dashed) lines, one (two) Λ is added to the ^{4}He nucleus. Three different functionals—from left to right DF-NSC89, DF-NSC97a, and DF-NSC97f—are considered.

and double-Λ densities (Fig. 6) show a moderate dependence on the model.

A definition of the average Λ density from the Λ-density profile is required to properly define the parameter $x_\Lambda(A)$. Figure 6 clearly shows that the Λ-density profile does not have a flat behavior at the center of a small hypernuclear system; as a consequence, the standard deviation from the average will be quite large. Table III displays the calculated average double-Λ densities and standard deviations for the same functionals as in Fig. 6, using three different ways to estimate the average Λ density,

$$\langle\rho_\Lambda\rangle_\Lambda = \frac{\int d^3r\ \rho_\Lambda\rho_\Lambda}{\int d^3r\ \rho_\Lambda}, \tag{41}$$

$$\langle\rho_\Lambda\rangle_N = \frac{\int d^3r\ \rho_\Lambda\rho_N}{\int d^3r\ \rho_N}, \tag{42}$$

$$\langle\rho_\Lambda\rangle_T = \frac{\int d^3r\ \rho_\Lambda\rho_T}{\int d^3r\ \rho_T}, \tag{43}$$

where $\rho_T = \rho_N + \rho_\Lambda$. The standard deviation is defined as $\sigma_i = \sqrt{\langle\rho_\Lambda^2\rangle_i - \langle\rho_\Lambda\rangle_i^2}$, with $i = \Lambda,\ N$, or T. The comparison between the different ways to extract the average Λ density in Table III shows a 15% deviation. As anticipated, the standard deviation is very large, almost of the order of the average value. It is therefore difficult to properly define an average Λ density in ${}^{6}_{\Lambda\Lambda}$He.

A general expression for the average Λ density in hypernuclei was given in Ref. [27], supposing that the Λ density scales with the nucleon density. A general expression [27] was therefore proposed,

$$\rho_\Lambda^{\text{general}}(A) \approx \Lambda\frac{\rho_0}{A}, \tag{44}$$

where $\Lambda = 1$ for single-Λ hypernuclei and $\Lambda = 2$ for double-Λ hypernuclei. Figure 7 shows the ratio of the microscopically calculated average Λ density $\langle\rho_\Lambda\rangle_T$ over the general expression (44). The general expression is rather well satisfied for large A, but a systematic deviation is observed for small A. The fit of the deviation is also shown in Fig. 7 and we obtain

$$\langle\rho_\Lambda\rangle_T \approx \rho_\Lambda^{\text{general}}(A)[0.957 - 2.54A^{-1}]. \tag{45}$$

This shows that Eq. (44) of Ref. [27] is not valid for $A \lesssim 50$. It should be noted that we have used the expression $\langle\rho_\Lambda\rangle_T$ [see Eq. (43)] as a reference to estimate the average Λ density. Similar results are obtained with $\langle\rho_\Lambda\rangle_N$ for large nuclei, but the definition $\langle\rho_\Lambda\rangle_\Lambda$ gives a systematic increase by a factor of about 2 compared to the two other definitions in large nuclei.

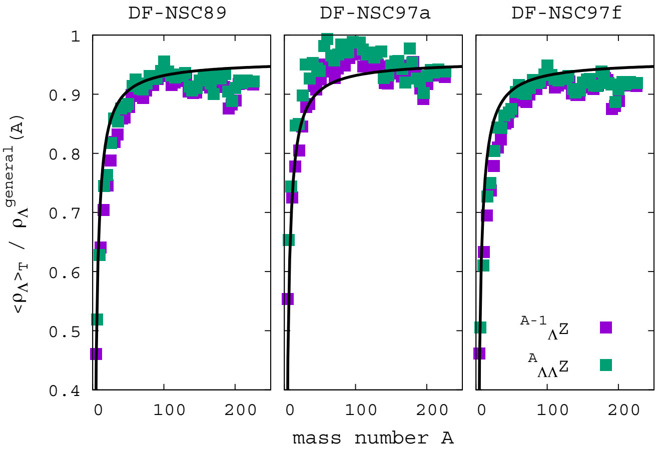

FIG. 7. (Color online) Ratios of the Λ density [Eq. (43)] over the approximate relation [Eq. (44)] as a function of baryon number for $\Lambda = 1$ (purple) and $\Lambda = 2$ (green). A fit is also shown. Three different functionals—from left to right DF-NSC89, DF-NSC97a, and DF-NSC97f—are considered.

B. Empirical determination of the term $\tilde{\epsilon}_{\Lambda\Lambda}$

The relation between the $\Delta B_{\Lambda\Lambda}(A)$ parameters and $x_\Lambda(A)$ is given by Eq. (17) for a given Λ hypernucleus A. However, while the bond energy can be determined from experimental mass measurements, the average Λ density has never been measured. We have seen in the previous section that the average Λ density depends on the functional and that the standard deviation in ${}^{6}_{\Lambda\Lambda}$He, the nucleus for which the best measurement of the bond energy exists [52,53], is almost comparable with the average Λ density. Two different methods are used to set the value of x_Λ.

EmpA: The value of $x_\Lambda({}^{6}_{\Lambda\Lambda}\text{He})$ is fixed to an average value (=1/6) in ${}^{6}_{\Lambda\Lambda}$He, independently of the functional.
EmpB: The value of x_Λ is optimized to obtain a fixed bond energy (≈1 MeV, consistent with Refs. [52,53] or ≈5 MeV, as suggested in Ref. [51]) in He for each functional.

In prescription EmpA, the relation between the bond energy and the functional is based on the local density approximation [see Eq. (17) and Appendix A for more details]. It is therefore interesting to calculate the bond energy which is obtained from the microscopic HF calculations to estimate the accuracy of the local density approximation. Doing so for DF-NSC89, DF-NSC97a, and DF-NSC97f, and varying the parameter x from 1/2 to 4, the difference between the bound energy set to determine the parameters and the one calculated from HF calculation in ${}^{6}_{\Lambda\Lambda}$He is less than 20%. A larger difference is found between the parameter $x_\Lambda = 1/6$ and the average Λ density in ${}^{6}_{\Lambda\Lambda}$He. We conclude that the the prescription EmpA, based on the local density approximation, cannot provide accurate parameters. This is related the analysis of the Λ density profile in ${}^{6}_{\Lambda\Lambda}$He, which is not flat enough to allow for the local density approximation (see Table III).

TABLE III. Calculations of average Λ densities in ${}^{6}_{\Lambda\Lambda}$He (in fm^{-3}) for the functionals DF-NSC89, DF-NSC97a, and DF-NSC97f.

	DF-NSC89	DF-NSC97a	DF-NSC97f
$10^2\langle\rho_\Lambda\rangle_\Lambda$	2.25	3.69	2.31
$10^2\langle\rho_\Lambda\rangle_N$	2.64	3.48	2.65
$10^2\langle\rho_\Lambda\rangle_T$	2.51	3.55	2.53
$10^2\sigma_\Lambda$	1.97	2.89	1.85
$10^2\sigma_N$	1.85	2.74	1.76
$10^2\sigma_T$	1.90	2.79	1.80

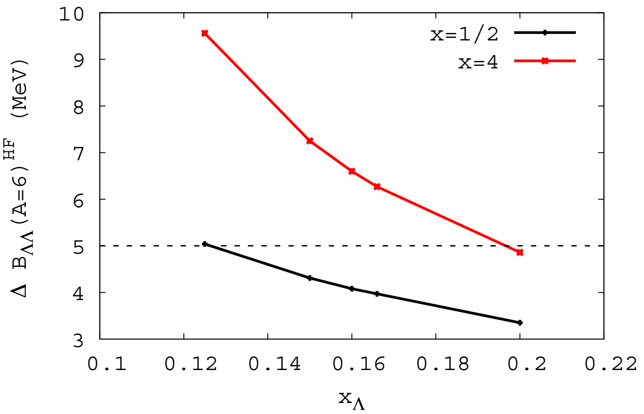

FIG. 8. (Color online) Relation between the parameter $x_\Lambda({}^{6}_{\Lambda\Lambda}\mathrm{He})$ and the bond energy set to 5 MeV [Eq. (16)] for He extracted from the HF calculation with the functional DF-NSC89 with $x = 1/2$ and DF-NSC89 with $x = 4$.

In the present approach, given by the prescription EmpB, the value of x_Λ is not fixed *a priori* but it is varied and correlated with the bond energy determined from the HF calculation. In such a way, the parameter x_Λ is treated as a variational parameter making it possible to fit the bond energy in He. The correlation between the parameter x_Λ and the bond energy $\Delta B_{\Lambda\Lambda}(A=6)^{\mathrm{HF}}$ is shown in Fig. 8 for the functional DF-NSC89 with $x = 1/2$ and DF-NSC89 with $x = 4$. The results for the functionals DF-NSC89, DF-NSC97a, and DF-NSC97f using this empirical prescription (called EmpB hereafter) are given in Table IV, obtained from the adjustment to the bond energy. Because a large arbitrariness is associated with the $\Lambda\Lambda$ functional, the simplest polynomial form that allows for the needed repulsion at high density, and corresponds to a bond energy of 1 MeV in ^{6}He and neighboring hypernuclei, is chosen. We therefore use the functionals of Table IV for the calculations of this work. Allowing for this large variation of the x parameter, the largely unknown behavior at supersaturation is therefore decoupled from the behavior at the very low densities implied for the hypernuclei.

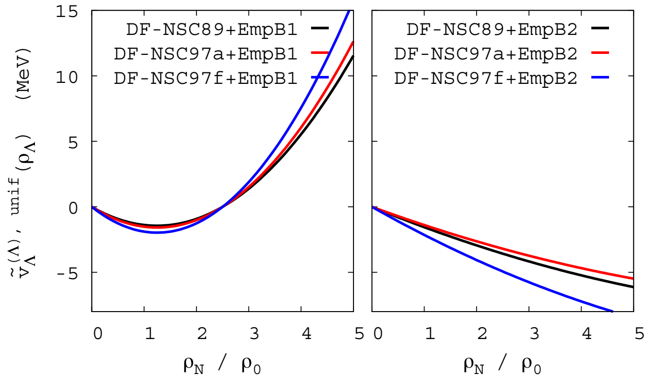

FIG. 9. (Color online) Comparison of the potential $v_\Lambda^{(\Lambda),\mathrm{unif}}(\rho_N,\rho_\Lambda)$ obtained with the prescription EmpB1 and EmpB2 (see legend) as a function of the nucleon density ρ_N (in units of the saturation density ρ_0) for the functionals DF-NSC89, DF-NSC97a, and DF-NSC97f. We have fixed $\Delta B_{\Lambda\Lambda} = 1$ MeV and the fraction of Λ to be 20%. In the left panel, we have fixed $x = 1/2$, while in the right, $x = 4$.

Finally, Fig. 9 compares the potentials $v_\Lambda^{(\Lambda),\mathrm{unif}}$ obtained from the functionals DF-NSC89, DF-NSC97a, and DF-NSC97f associated with the empirical prescriptions EmpB1 and EmpB2, where the bond energy is fixed to 1 MeV. Around saturation density, the different models shown in Fig. 9 predict negative values ranging from -1 to -2 MeV. At densities higher than normal nuclear saturation density, the prescription EmpB1 makes the potential $v_\Lambda^{(\Lambda),\mathrm{unif}}$ much stiffer than the prescription EmpB2. It is also interesting to compare the empirical models shown in Fig. 9 with the initial ones displayed in Fig. 2: The empirical prescription EmpB1 produces the stiffest potential, while EmpB2 the softest. Our empirical prescription increases the exploratory domain of variation for the $\Lambda\Lambda$ potential, as well as includes the initial potential.

C. Calculations in Λ hypernuclei

In the following, we consider the three functionals—DF-NSC89, DF-NSC97a, and DF-NSC97f—corrected with

TABLE IV. Prescription EmpB. We present the adjustment of the parameter $x_\Lambda(4)$ to the bond energy (≈1 or 5 MeV in ^{4}He), the values of the parameters $\tilde{\alpha}_7^B$ and $\tilde{\alpha}_8^B$, and the ratio of the Λ density to the saturation density in He.

Potential ΛN Potential $\Lambda\Lambda$ x	DF-NSC89 EmpB1 1/2	DF-NSC89 EmpB2 4	DF-NSC97a EmpB1 1/2	DF-NSC97a EmpB2 4	DF-NSC97f EmpB1 1/2	DF-NSC97f EmpB2 4
			$\Delta B_{\Lambda\Lambda}(A=6) = 5$ MeV			
$\tilde{\alpha}_7$	150	80.82	150	70.64	160.48	100.33
$\tilde{\alpha}_8$	1250	84.19	1250	73.59	1337	104.51
$\Delta B_{\Lambda\Lambda}(6)^{\mathrm{HF}}$	5.05	4.86	5.17	5.03	4.84	5.00
x_Λ	0.125	0.2	0.125	0.23	0.115	0.16
			$\Delta B_{\Lambda\Lambda}(A=6) = 1$ MeV			
$\tilde{\alpha}_7$	36.05	25.53	39.46	22.85	49.24	35.25
$\tilde{\alpha}_8$	300.48	26.60	328.81	23.81	410.32	36.72
$\Delta B_{\Lambda\Lambda}(6)^{\mathrm{HF}}$	0.97	1.1	0.95	1.04	0.98	1.05
x_Λ	0.1	0.125	0.09	0.14	0.07	0.09

the empirical prescriptions EmpB1 and EmpB2 associated with a bond energy of 1 MeV. We therefore consider six $N\Lambda + \Lambda\Lambda$ functionals, corresponding to Table IV, together with SLy5 [39] for the NN functional. For each $N\Lambda$ functional (DF-NSC89, DF-NSC97a, and DF-NSC97f), the first one (e.g., DF-NSC89-EmpB1) corresponds to the lowest hyperon density in nuclear matter ($x = 1/2$), whereas the second one (e.g., DF-NSC89-EmpB2) corresponds to the largest hyperon density ($x = 4$).

It should be noted that the present work is focused on the uncertainty generated by the Λ related functionals on the number of bound systems. The uncertainties generated by the NN functional itself have already been studied on the nuclear chart and is typically of 7% on the number of bound nuclei [32].

In the present work, the Λ-hypernuclear charts are calculated for even-even-even Λ hypernuclei. Because spherical symmetry is imposed, only magic Λ number Λ hypernuclei are considered. It should be noted that a fully microscopic deformed approach such as Ref. [8] is the most accurate one to predict driplines. However, such a task is numerically very demanding, and it is beyond the scope of the present paper.

As mentioned above, the spin-orbit interaction is known to be weak in the Λ channel [38], a factor 100 lower than in the nucleonic sector [54], according to experimental data. The Λ magic numbers are therefore expected to be close to the harmonic oscillator ones: 2, 8, 20, 40, and 70. Calculations are performed for Λ-hypernuclear charts corresponding to these specific numbers of Λ.

IV. THE Λ HYPERDRIPLINES

The Λ hyperdripline has been studied in Ref. [26] with a similar HF approach, showing that the maximum number of bound Λ in a hypernucleus is about 1/3 of the number of nucleons. We aim here to provide a more general study of hyperdriplines, namely also showing the evolution of the proton and neutron driplines with the number of hyperons. It is important to stress that driplines associated with a Λ fraction $\rho_\Lambda/\rho_N \approx 0.17$ have to be considered as a lower bound, because even more strangeness would be compatible with bound systems if Ξ, which are neglected in the present approach, were accounted for.

Figure 10 displays the microscopically calculated Λ-hypernuclear charts for $\Lambda = 0$, 2, 8, 20, 40, and 70 using the DF-NSC89 + EmpB1 functional. Adding Λ's to a nucleus increases the binding energy for $\Lambda < 40$, but conversely decreases it for $\Lambda = 40$ and 70. This is attributable to the balance between the attractive ΛN and $\Lambda\Lambda$ functionals and the progressive energy filling of the Λ states in the mean Λ potential. Figure 10 also shows that with a large number of Λ's, the corresponding hypernuclear chart is shifted towards larger N, Z values. This effect is mainly attributable to the ΛN functional and is related to the maximum fraction of 1/3 of hyperons with respect to nucleons, as mentioned above. For instance, the exotic ^{190}Th core becomes bound in the presence of 70 Λ. A similar stabilization of exotic nuclear core has been predicted in Ref. [18].

To get a more accurate estimation of the dripline, Fig. 11 displays the dripline neutron numbers for each Z value in the case of $\Lambda = 20$ and for the six ($\Lambda\Lambda + \Lambda N$) functionals that we consider. The dripline is here defined when the chemical potential becomes positive. The results are rather similar among the various functionals. This shows that, despite the very large differences among these functionals, in both the $N\Lambda$ and the $\Lambda\Lambda$ channels, the error bars are not so large for the dripline determination, contrary to what could be expected. This may be attributable to the narrower density range corresponding to finite hypernuclei compared to hypernuclear matter, because the six functionals provide similar potentials for subsaturation densities.

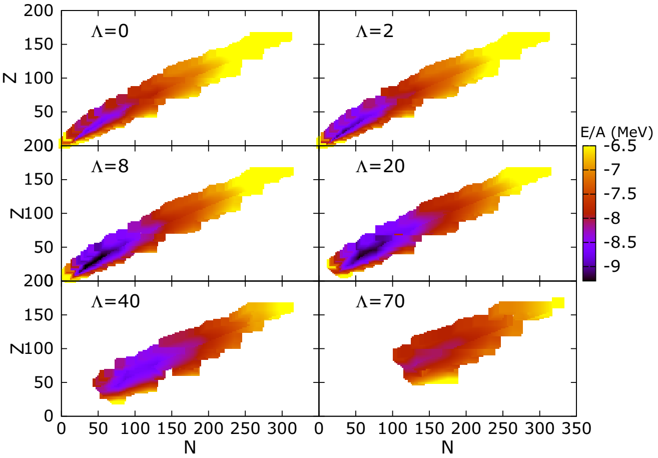

FIG. 10. (Color online) Λ-hypernuclear charts for magic Λ numbers calculated with the DF-NSC89 + EmpB1 functional.

The number of bound even-even-even Λ hypernuclei found for $\Lambda \leqslant 70$ and $Z \leqslant 120$ are given in Table V. The dispersion owing to the uncertainty on the Λ-related functional is rather small: The average total number of even-even-even hypernuclei for $\Lambda = 0, 2, 8, 20, 40$, and 70 is 9770 ± 429. Interpolating the number of even-even-even hypernuclei on the whole hypernuclear chart, provides 59 538 ± 4020 hypernuclei with a larger relative systematic uncertainties, which can be inferred

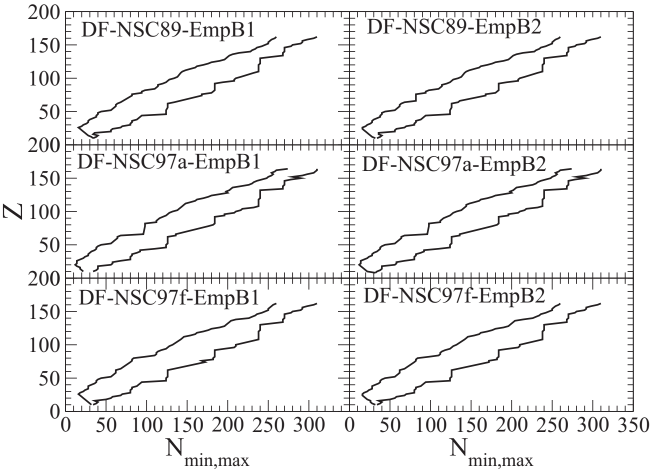

FIG. 11. Minimal (upper line) and maximal (lower line) neutron number value for hypernuclei with $\Lambda = 20$ using the six functionals described in Table IV.

TABLE V. Number of bound even-even-even Λ hypernuclei for Λ < 70 and $Z < 120$.

No. of nuclei	DF-NSC89 +EmpB1	DF-NSC89 +EmpB2	DF-NSC97a +EmpB1	DF-NSC97a +EmpB2	DF-NSC97f +EmpB1	DF-NSC97a +EmpB2
$\Lambda = 0$	1578	1578	1573	1573	1578	1578
$\Lambda = 2$	1628	1640	1617	1619	1634	1621
$\Lambda = 8$	1647	1644	1692	1680	1750	1749
$\Lambda = 20$	1650	1681	1696	1724	1675	1683
$\Lambda = 40$	1713	1736	1961	1972	1722	1716
$\Lambda = 70$	1162	1237	1746	1886	1127	1152
Total	9378	9516	10 285	10 454	9486	9499
Total interpolated	56 140	57 287	64 459	65 587	56 646	56 809

from the interpolation procedure. The interpolation is linearly performed between the calculated magic Λ hypercharts.

We stress that this interpolation is only done with the purpose of estimating of the total number of bound systems. To have a detailed description of the nonmagic hypernuclear chart, taking into account deformations would be essential [8].

The corresponding uncertainty is calculated from the dispersion of the total number of even-even-even hypernuclei obtained with the six (ΛΛ + ΛN) functionals. It should also be noted that magic nuclei are specific nuclei in the hypernuclear channel and therefore the interpolation procedure is not optimal. Considering the uncertainty on the bond energy (between 1 and 5 MeV, as explained in the previous section), the number of estimated even-even-even nuclei is 61 460 ± 4300. The total number of hypernuclei, considering the odd ones is therefore 491 680 ± 34 400. If the uncertainty of the NN functional [32] is included (here in a decorrelated way), the total number of hypernuclei with $\Lambda \leqslant 70$ and $Z \leqslant 120$ is 491 680 ± 59 000.

The relative uncertainty is therefore of about 4% on the magic Λ-hypernuclear charts. It is determined using the mean value and the corresponding standard deviation considering the six (ΛN + ΛΛ) functionals. It should be noted that the DF-NSC97a functional is more attractive than the other functionals, which is the main contribution to the uncertainties on the number of bound hypernuclei. If the bond energy requirement is changed from 1 to 5 MeV, the variation among the six newly derived functionals is about 5%. All in all, it is safe to consider an upper limit of 7% uncertainty owing to the ΛΛ and the ΛN functionals on the magic Λ hypernuclear charts. In the case of interpolated values, the uncertainty is of about 7% considering the six (ΛN + ΛΛ) functionals, plus 5% from changing the bond energy requirement from 1 to 5 MeV. These values should be compared to the relative uncertainty of about 7% when the NN Skyrme functional is changed [32] on the nuclear chart. It shows that the uncertainty from the Λ-related functionals is not significantly larger than the one from the NN functional. This is attributable to the focused range of densities (i.e., below the saturation one) relevant for hypernuclei, as mentioned above.

Coming back to the sensitivity of the hyperdriplines to the $\Lambda + \Lambda \rightarrow N + \Xi$ decay channel, we mention that within the generalized liquid-drop model proposed by Samanta [24] and straightforward to use it comes out that the n-rich frontier is almost unaffected by considering Ξ's in addition to Λs while the neutron-poor frontier is shifted to lower N values. Quite remarkable, according to Ref. [24] along the n-poor dripline strangeness consists almost entirely out of Ξ^-, while along the n-rich dripline strangeness is to a large extent made of Λs. The broadening of the hypernuclear chart is proportional with the strangeness fraction. The same qualitative behavior is expected to manifest also in the case of the present model.

V. Λ-HYPERNUCLEAR STRUCTURE

A. Binding energy: Fusion and fission of Λ hypernuclei

It may be relevant to study how the presence of hyperons impacts the most bound hypernuclei per baryon, which is known to be in the Fe-Ni region in the case of nuclei.

Figure 12 displays the evolution of the largest B/A value as a function of the number of hyperons in hypernuclei calculated with four (ΛN + ΛΛ) functionals. A remarkable agreement between the four functionals considered is observed, which may suggests that the theoretical uncertainty on the problem of hypernuclear binding is relatively under control, at least in the low-density region corresponding to nuclei. It would be very interesting to know if this agreement is kept using relativistic functionals as in Ref. [29]. In the case of DF-NSC89 + EmpB1 and for $\Lambda = 2$ or 8, the optimal Z value is not much changed

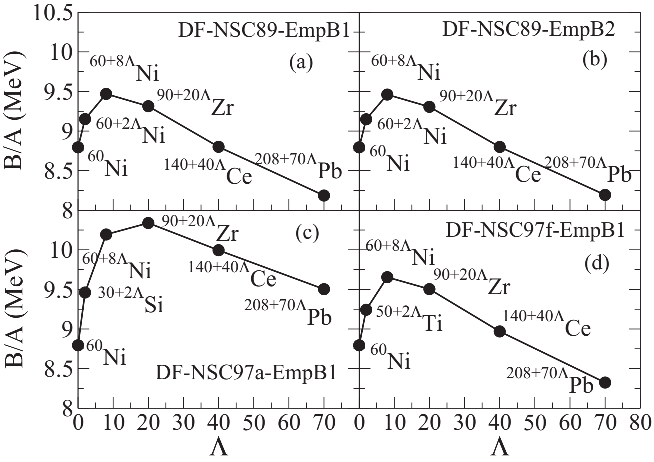

FIG. 12. Λ hypernuclei with maximum binding energy per baryon as a function of Λ for the DF-NSC89 + EmpB1 (a), DF-NSC89 + EmpB2 (b), DF-NSC97a + EmpB1 (c), DF-NSC97f + EmpB1 (d) functionals.

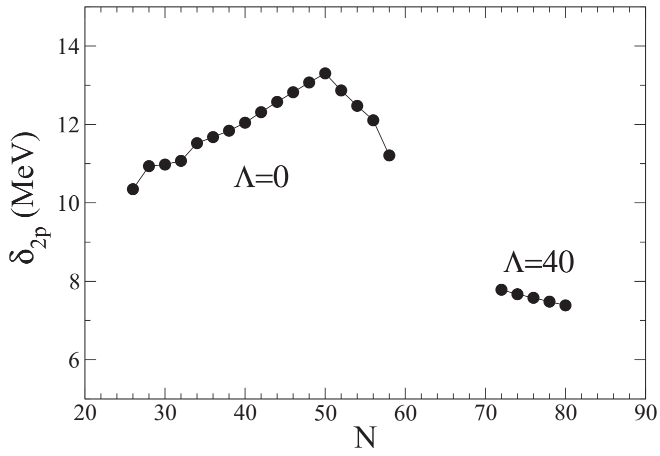

FIG. 13. The two protons gap in the bound nickel isotopes for $\Lambda = 0$ and $\Lambda = 40$, defined as $\delta_{2p} \equiv S_{2p}(A,Z) - S_{2p}(A+2,Z+2)$, calculated with the DF-NSC89 + EmpB1 functional.

compared to the nickel-iron area. For a number of hyperons from 20 and larger the most bound hypernucleus is obtained for larger Z, typically for Zr, Ce, and Pb. The results are qualitatively similar with the other functionals, except in the case of DF-NSC97a + EmpB1 and DF-NSC97f + EmpB1, for 2Λ hypernuclei: The addition of only 2Λ makes Si and, respectively, Ti the most bound nucleus in terms of binding energy per baryon. This result shows the non-negligible impact of hyperons on the binding energy of the system.

B. Magicity

Several signals of the evolution of the magic gaps along the nuclear chart have been obtained these past decades [55]. It may therefore be relevant to extend prediction of magicity to the hypernuclear chart. The two protons or two neutrons gap are known to be a relevant quantity to provide a first insight on magicity features in nuclei.

It is known that shell effects can vanish in the case of very neutron-rich nuclei [56,57] because of the smoothness of the neutron skin triggering a weakening of the spin-orbit effect and therefore its corresponding magic numbers. This is the case for hypernuclei with a low number of Λ. However, in the case of $\Lambda = 40$, Fig. 13 shows a restoration of the $Z = 28$ magicity for the very neutron-rich hypernickels with $70 < N < 80$: The spin-orbit weakening of the $Z = 28$ magic number for very neutron-rich hypernuclei is reduced by the presence of hyperons. A similar effect is observed for $\Lambda = 70$ and the $N = 186$ magic number: It is restored for $82 < Z < 98$. The present results were obtained with DF-NSC89 + EmpB1 and similar results are obtained with the other functionals. A weakening of the $N = 28$ shell closure is found for $\Lambda < 8$, in agreement with the previous results. Also a $Z = 40$ weakening is observed for these hypernuclei.

Figure 14 displays the neutron, proton, and hyperon densities for the triply magic hypernucleus $^{208+\Lambda}$Pb with $\Lambda = 2$, 8, 20, 40, and 70. The proton and neutron densities are almost not impacted by the hyperon addition, showing a relative independence of the hyperons with respect to the nucleonic

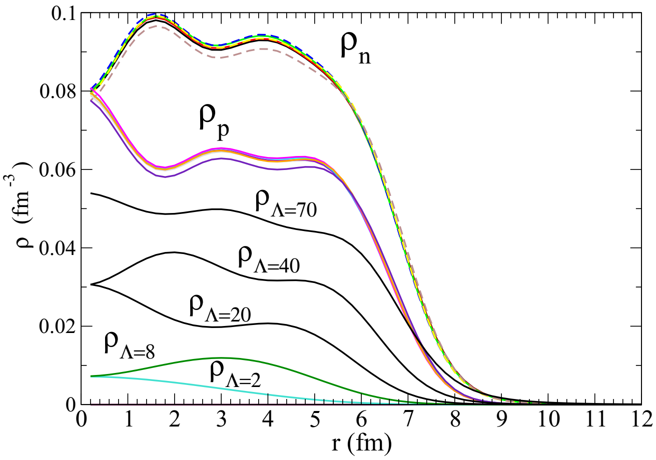

FIG. 14. (Color online) Baryonic densities for the triply magic $^{208+\Lambda}$Pb hypernucleus with $\Lambda = 2$, 8, 20, 40, 70.

core. The results are in agreement with Ref. [26], where the Skyrme parametrization SIII was used and the $\Lambda\Lambda$ functional neglected. Qualitative agreement, that is stability of radial nucleonic mass distribution and nonmonotonic evolution of strangeness radial distributions upon increasing the number of Λ's, is also obtained with the pioneering work of Ref. [14], where double and triple magic O and Ca hypernuclei have been addressed within a relativistic mean-field (RMF) model. This validates the present approach and more globally the microscopic prediction of hypernuclei properties.

C. Bubbles and halos

Bubble and halo effects have recently been studied in Λ hypernuclei [29]. Hyperons are more diffuse in a nucleus than nucleons. This could be attributable to the weaker $\Lambda\Lambda$ attraction compared to the NN one, generating a hyperon saturation density about 1/3 smaller than the nucleonic one. This may also be attributable to the $\Lambda\Lambda$ functional, which is much more intense in Ref. [29] than the one used in the present work. It emphasizes the importance of taking into account the bond energy to constrain the $\Lambda\Lambda$ functional, as depicted in Secs. II and III.

It is well known that the addition of a single-Λ hyperon shrinks the nuclear core [58], both from predictions and from measurements. It is therefore relevant to study the effect on the neutron and proton densities of a large number of hyperons. We find no large effect of the increase of the Λ number on the proton nor on the neutron density in ^{16}O. In the case of $^{104+40\Lambda}$Cr, the Λ's act like a glue between protons and neutrons and even drive the proton to larger radii, as shown by Fig. 15. A similar effect is observed on the neutron density. This is attributable to the fact that hyperons attract nucleons at larger radii. It should also be noted that the halo effect in $^{104+40\Lambda}$Cr is rather small compared to predictions using RMF approaches [29].

In the case of bubbles [29,59,60], there is no strong impact of the increase of number of hyperons on the depletion. Figure 16 displays the proton, neutron, and hyperon densities in ^{34}Si with no hyperons and the addition of two and eight

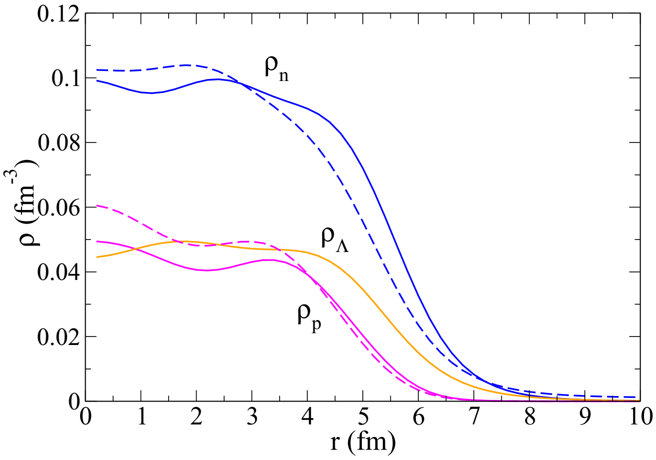

FIG. 15. (Color online) Baryon densities for the magic $^{144}\mathrm{Cr}_{40\Lambda}$ hypernucleus (solid lines). The neutron and proton densities for the ^{104}Cr nucleus are shown as dashed lines.

hyperons. As described above, the proton and neutron densities are almost not impacted by the addition of hyperons and therefore the predicted proton depletion in ^{34}Si remains. This small interdependence is at variance with relativistic calculations obtained with the RMF approach [29].

In summary, the present results show that the effect of Λ hyperons on the nucleon core is much weaker than in the RMF case. This may be attributable to the different $(N\Lambda + \Lambda\Lambda)$ functionals that are used in the two approaches, as well as to the Fock term, which is not considered in the RMF case [37]. It should be noted that the present $(N\Lambda + \Lambda\Lambda)$ functionals are constrained with bond energy requirements.

VI. CONCLUSIONS

In this work, we have investigated the relations between Λ-hyperonic data (at low Λ density), and high-density properties. For that we have proceeded in two steps. First we have discussed the properties of the functionals, based on BHF data, and proposed an empirical prescription for the $\Lambda\Lambda$ term. Then we have explored the hypernuclear chart allowing the functional to vary inside our domain of uncertainty.

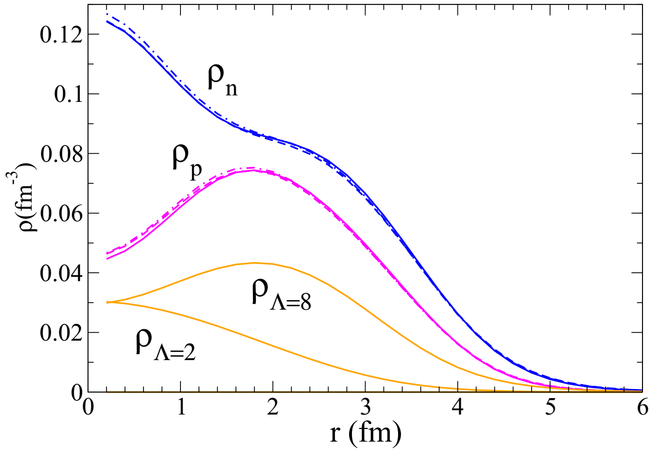

FIG. 16. (Color online) Baryon densities for $^{34+\Lambda}$Si hypernucleus with $\Lambda = 2$ (dot-dashed lines for neutron and proton densities) and $\Lambda = 8$ (solid lines). The neutron and proton densities for the ^{34}Si nucleus are shown as dashed lines.

In the first step, we found that the low-density part of the functional is well determined by the value of the bond energy, while the high-density part is determined by the unique free parameter of the model, which controls the density at which the $\Lambda\Lambda$ term changes its sign. As such, we show that the bond energy controls the low-density part of the EoS solely. This means that hypernuclear data cannot be used to determine the high-density behavior of hyperonic matter, and other constraints from neutron star physics or heavy-ion data are needed in that region. This general conclusion is certainly independent of our model and shall be found also in other approaches.

In the second step, the Λ-hypernuclear chart for even-even-even hypernuclei with $Z \leqslant 120$ and $\Lambda = 2$, 8, 20, 40, and 70 has been calculated using the Hartree-Fock method with Skyrme NN functional and designed $N\Lambda$ and $\Lambda\Lambda$ functionals. Six $(N\Lambda + \Lambda\Lambda)$ functionals were used, optimized such as to reproduce the present experimental constraint of a bond energy of 1 MeV. The position of the Λ hyperdriplines is determined with a 7% accuracy, with comparable contribution from the uncertainty on the NN functionals and on the Λ related functionals. The number of such bound even-even-even Λ hypernuclei is estimated to 9770 ± 429, leading to an estimation of the total number of Λ hypernuclei with $\Lambda < 70$ and $Z < 120$ of $491\,680 \pm 59\,000$.

Significant deviations from iron-nickel elements can be found for Λ hypernuclei with the largest binding energy per baryon, especially for $\Lambda \geqslant 20$. The spin-orbit weakening of the neutron magicity close to the neutron dripline is quenched by the presence of hyperons. The nucleonic-core profile is not much affected by the presence of hyperons, allowing for the persistence of the proton bubble in ^{34}Si with additional hyperons.

The present results shall benefit from the more and more accurate design of the Λ-based functionals. The measurements of Λ and multi-Λ hypernuclei, Λ-density profiles, as well as Λ-Ξ and Ξ-Ξ interactions, would greatly help to provide such critical information.

ACKNOWLEDGMENTS

The authors thank I. Vidaña for fruitful discussions. This work has been partially funded by the SN2NS Project No. ANR-10-BLAN-0503 and it has been supported by New-Compstar, COST Action No. MP1304 and the Institut Universitaire de France.

APPENDIX A: RELATION BETWEEN THE BOND ENERGY AND THE FUNCTIONAL

For a nucleus hereafter called $(A-1)$, including one Λ and $A-2$ nucleons, its total energy can be approximatively given by

$$E\left({}^{A-1}_{\Lambda}Z\right) \approx E\left({}^{A-2}Z\right) + e_\Lambda(A-1), \tag{A1}$$

where $e_\Lambda(A-1)$ is the single-particle energy of the Λ state in the ${}^{A-1}_{\Lambda}Z$ hypernucleus, taking into account only the $N\Lambda$ interaction. For the double-Λ ${}^{A}_{\Lambda\Lambda}Z$ hypernucleus, we have also

$$E\left({}^{A}_{\Lambda\Lambda}Z\right) \approx E({}^{A-2}Z) + 2e_\Lambda(A) + U_\Lambda^{(\Lambda)}[\rho_\Lambda(A)], \tag{A2}$$

where $U_\Lambda^{(\Lambda)}[\rho_\Lambda(A)]$ is the Λ potential term induced by the presence of Λ particles. In the present functional approach, we remind the reader that the momentum dependence of the $\Lambda\Lambda$ interaction is neglected and that $U_\Lambda^{(\Lambda)}$ is momentum independent. Using the local density approximation, it is a function of the average Λ density in the ${}^{A}_{\Lambda\Lambda}Z$ hypernucleus, $\rho_\Lambda(A)$. From the BHF framework, it can be shown that [27]

$$\epsilon_{\Lambda\Lambda} = \tfrac{1}{2}\rho_\Lambda U_\Lambda^{(\Lambda)}. \tag{A3}$$

Inserting Eqs. (A1) and (A2) into Eq. (16), the bond energy reads

$$\Delta B_{\Lambda\Lambda}(A) \approx 2e_\Lambda(A-1) - 2e_\Lambda(A) - U_\Lambda^{(\Lambda)}[\rho_\Lambda(A)]. \tag{A4}$$

It should be noted that, to obtain Eq. (A4), we have assumed the independent particle approximation. Because the momentum dependence of $U_\Lambda^{(\Lambda)}$ is neglected, the Λ-effective mass is the same in double-Λ and single-Λ hypernuclei and depend only on ρ_N as in Eq. (34). The difference $e_\Lambda(A-1) - e_\Lambda(A)$, which is mostly induced by the rearrangement term in the mean field, is calculated to be small. We therefore approximate $e_\Lambda(A-1) \approx e_\Lambda(A)$ to obtain

$$\Delta B_{\Lambda\Lambda}(A) \approx -U_\Lambda^{(\Lambda)}[\rho_\Lambda(A)] = -2\frac{\epsilon_{\Lambda\Lambda}[\rho_\Lambda(A)]}{\rho_\Lambda(A)}, \tag{A5}$$

where Eq. (A3) has been used.

APPENDIX B: STRANGENESS ANALOG RESONANCES

Strangeness analog resonances (SARs) are similar to isobaric analog states, with the transformation of a nucleon into an hyperon instead of a transformation of, e.g., a neutron into a proton. In Ref. [61], Kerman and Lipkin studied the SAR states between nuclei and excited states of single-hyperon hypernuclei. It is interesting to generalize this approach to multi-Λ systems.

Kerman and Lipkin assumed that the energy difference (the degeneracy raising) between a nucleus and the corresponding hypernucleus state where a neutron is replaced by an hyperon is attributable to (i) the mass difference between the Λ and the neutron and (ii) the difference between the nucleonic and the hyperonic potentials [61],

$$\Delta E(\mathrm{SAR}) \equiv m\left({}^{A}X^*_\Lambda\right) - m({}^{A}X) = (V_{0\Lambda} - V_{0n}) + (m_\Lambda - m_n), \tag{B1}$$

where $\mathrm{V}_{0\Lambda}$ and V_{0n} are the depth of the hyperon and nucleons potentials, respectively, and $\Lambda = 1$ here.

This corresponds to an excitation energy in the hypernucleus of

$$E^* \equiv m\left({}^{A}X^*_\Lambda\right) - m\left({}^{A}X_\Lambda\right) = -S_n({}^{A}X) + (V_{0\Lambda} - V_{0n}) + B_\Lambda, \tag{B2}$$

where B_Λ is the binding energy of the hyperon in the single-Λ hypernucleus and $\mathrm{S}_n({}^{A}X)$ the one neutron separation energy of the ${}^{A}X$ nucleus.

The questions arises as to whether the above relation can be generalized to multi-Λ nuclei. A straightforward derivation makes it possible to derive the mass (namely, the excited state) of the hypernucleus having Λ hyperons from the mass of the initial nucleus,

$$\Delta E(\mathrm{SAR}) = \Lambda[(V_{0\Lambda} - V_{0n}) + (m_\Lambda - m_n)], \tag{B3}$$

where $\Lambda \geqslant 1$. It should be noted that the $\Lambda\Lambda$ interaction is neglected here, as well as rearrangement terms. This could result in a significant different form of Eq. (B3). However, as shown below, the energy position of SAR states will mainly be impacted by the nucleon vs Λ mass difference.

Equation (B3) shows that the SAR states in multihyperons are expected to display a rather harmonic spectrum, because the last term in brackets of the right-hand side remains rather constant: There is about 30 MeV difference between the neutron and the hyperon mean potentials [26] and 170-MeV difference between the neutron and the hyperon masses:

$$m\left({}^{A}X^*_\Lambda\right) \simeq m({}^{A}X) + \Lambda.200\ \mathrm{MeV}. \tag{B4}$$

It should be noted that this 200-MeV constant value originates from the saturation properties in hypernuclei, which, in turn, leads to a constant difference between the nucleon and the hyperon potentials. Moreover, in the corresponding hypernuclei, these states would correspond to excited states located around Λ.30 MeV, which becomes unbound already for small value of Λ. In summary, the SAR states have been generalized to multihyperon hypernuclei. They shall not correspond to bound states for most of them, but to resonances embedded in the continuum.

---

[1] A. R. Bodmer and S. Ali, Nucl. Phys. **56**, 657 (1964).

[2] R. H. Dalitz and A. Gal, Phys. Rev. Lett. **36**, 362 (1976); Phys. Lett. B **64**, 154 (1976).

[3] D. J. Millener, C. B. Dover, and A. Gal, Phys. Rev. C **38**, 2700 (1988).

[4] M. Rayet, Ann. Phys. **102**, 226 (1976); Nucl. Phys. A **367**, 381 (1981).

[5] N. Auerbach, N. Van Giai, and S. Y. Lee, Phys. Lett. B **68**, 225 (1977); N. Van Giai, Invited talk at the International Topical Conference on Meson-Nuclear Physics, Pittsburg (1976); N. Auerbach and N. Van Giai, Phys. Lett. B **90**, 354 (1980).

[6] D. E. Lanskoy, Phys. Rev. C **58**, 3351 (1998).

[7] J. Meng, H. Toki, S. G. Zhou *et al.*, Prog. Part. Nucl. Phys. **57**, 470 (2006).

[8] Xian-Rong Zhou, H.-J. Schulze, H. Sagawa, C.-X. Wu, and E.-G. Zhao, Phys. Rev. C **76**, 034312 (2007).

[9] H. F. Lü, Chin. Phys. Lett. **25**, 3613 (2008).

[10] N. Guleria, S. K. Dhiman, and R. Shyam, Nucl. Phys. A **886**, 71 (2012).

[11] F. Minato and K. Hagino, Phys. Rev. C **85**, 024316 (2012).

[12] A. Bouyssy, Nucl. Phys. A **381**, 445 (1982).

[13] M. Rufa, H. Stoecker, J. A. Maruhn, W. Greiner, and P. G. Reinhard, J. Phys. G **13**, L143 (1987).

[14] J. Mares and J. Zofka, Z. Phys. A **333**, 209 (1989).

[15] M. Rufa, J. Schaffner, J. Maruhn, H. Stöcker, W. Greiner, and P.-G. Reinhard, Phys. Rev. C **42**, 2469 (1990).

[16] J. Schaffner, C. Greiner, and H. Stöcker, Phys. Rev. C **46**, 322 (1992).

[17] J. Mares and J. Zofka, Z. Phys. A **345**, 47 (1993).

[18] J. Schaffner, C. B. Dover, A. Gal *et al.*, Ann. Phys. **235**, 35 (1994).

[19] E. N. E. Van Dalen, G. Colucci, and A. D. Sedrakian, Phys. Lett. B **734**, 383 (2014).

[20] S. Balberg, A. Gal, and J. Schaffner, Prog. Theor. Phys. Suppl. **117**, 325 (1994).

[21] C. B. Dover and A. Gal, Nucl. Phys. A **560**, 559 (1993).

[22] C. Samanta, P. Roy Chowdhury and D. N. Basu, J. Phys. G: Nucl. Part. Phys. **32**, 363 (2006).

[23] C. Samanta, P. Roy Chowdhury, and D. N. Basu, J. Phys. G: Nucl. Part. Phys. **35**, 065101 (2008).

[24] C. Samanta, J. Phys. G: Nucl. Part. Phys. **37**, 075104 (2010).

[25] D. E. Lanskoy and Y. Yamamoto, Phys. Rev. C **55**, 2330 (1997).

[26] J. Cugnon, A. Lejeune, and H.-J. Schulze, Phys. Rev. C **62**, 064308 (2000).

[27] I. Vidaña, A. Polls, A. Ramos, and H.-J. Schulze, Phys. Rev. C **64**, 044301 (2001).

[28] F. Minato and K. Hagino, Phys. Rev. C **88**, 064303 (2013).

[29] M. Ikram, S. K. Singh, A. A. Usmani, and S. K. Patra, Int. J. Mod. Phys. E **23**, 1450052 (2014).

[30] H. Y. Sang, X. S. Wang, J. H. Wang, and H. F. Lü, Eur. Phys. J. A **50**, 52 (2014).

[31] W. Greiner, *Lecture Notes in Physics*, edited by J. M. Arias and M. Lozano (Springer-Verlag, Berlin, 2001), Vol. 581.

[32] J. Erler, N. Birge, M. Kortelainen, W. Nazarewicz, E. Olsen, A. M. Perhac, and M. Stoitsov, Nature (London) **486**, 509 (2012).

[33] P.-G. Reinhard and W. Nazarewicz, Phys. Rev. C **87**, 014324 (2013).

[34] Wei-Chia Chen and J. Piekarewicz, Phys. Rev. C **90**, 044305 (2014).

[35] J. Schaffner-Bielich and A. Gal, Phys. Rev. C **62**, 034311 (2000).

[36] P. Khaustov *et al.*, Phys. Rev. C **61**, 054603 (2000).

[37] E. Massot, J. Margueron, and G. Chanfray, Eur. Phys. Lett. **97**, 39002 (2012).

[38] P. Finelli, N. Kaiser, D. Vretenar, and W. Weise, Phys. Lett. B **658**, 90 (2007); Nucl. Phys. A **831**, 163 (2009).

[39] E. Chabanat, P. Bonche, P. Haensel, J. Meyer, and R. Schaeffer, Nucl. Phys. A **635**, 231 (1998).

[40] H.-J. Schulze and T. Rijken, Phys. Rev. C **88**, 024322 (2013).

[41] P. M. M. Maessen, T. A. Rijken, and J. J. de Swart, Phys. Rev. C **40**, 2226 (1989).

[42] T. A. Rijken, V. G. J. Stoks, and Y. Yamamoto, Phys. Rev. C **59**, 21 (1999).

[43] V. G. J. Stoks and T. A. Rijken, Phys. Rev. C **59**, 3009 (1999).

[44] J. Bartel, K. Bencheikh, and J. Meyer, Phys. Rev. C **77**, 024311 (2008).

[45] M. Bender, P.-H. Heenen, and P.-G. Reinhard, Rev. Mod. Phys. **75**, 121 (2003).

[46] V. G. J. Stoks and T. S. H. Lee, Phys. Rev. C **60**, 024006 (1999).

[47] S. Weissenborn, D. Chatterjee, and J. Schaffner-Bielich, Phys. Rev. C **85**, 065802 (2012).

[48] M. Oertel, C. Providência, F. Gulminelli, and Ad. R. Raduta, J. Phys. G **42**, 075202 (2015).

[49] P. B. Demorest, T. Pennucci, S. M. Ransom, M. S. E. Roberts, and J. W. T. Hessels, Nature (London) **467**, 1081 (2010).

[50] G. Colucci and A. Sedrakian, Phys. Rev. C **87**, 055806 (2013).

[51] G. B. Franklin, Nucl. Phys. A **585**, 83c (1995).

[52] S. Aoki *et al.*, Nucl. Phys. A **828**, 191 (2009).

[53] J. K. Ahn *et al.*, Phys. Rev. C **88**, 014003 (2013).

[54] O. Hashimoto and H. Tamura, Prog. Part. Nucl. Phys. **57**, 564 (2006), and references therein.

[55] M.-G. Porquet and O. Sorlin, Prog. Part. Nucl. Phys. **61**, 602 (2008).

[56] J. Dobaczewski, I. Hamamoto, W. Nazarewicz, and J. A. Sheikh, Phys. Rev. Lett. **72**, 981 (1994).

[57] D. Peña Arteaga, E. Khan, and P. Ring, Phys. Rev. C **79**, 034311 (2009).

[58] K. Tanida *et al.*, Phys. Rev. Lett. **86**, 1982 (2001), and references therein.

[59] E. Khan, M. Grasso, J. Margueron, and N. Van Giai, Nucl. Phys. A **800**, 37 (2008).

[60] M. Grasso, L. Gaudefroy, E. Khan, T. Nikšić, J. Piekarewicz, O. Sorlin, N. Van Giai, and D. Vretenar, Phys. Rev. C **79**, 034318 (2009).

[61] A. K. Kerman and H. J. Lipkin, Ann. Phys. **66**, 738 (1971).